the order of V, i.e., equilibrium ionization is achieved at the exit plane for all $C_r > C_{r,\text{crit}}$. (The discontinuities in Fig. 2 are, of course, a consequence of the sudden freeze approximation. Actually, each transition will be continuous[3] but quite abrupt.) The ordering and separation between the V/RT_e contours in the nonequilibrium region of Fig. 2 have two important implications. First, they indicate that a correlation of log a_j vs T_j^{-1} will exhibit greater curvature (concave upward) in the nonequilibrium regime than in either the frozen flow or equilibrium extremes. However, depending upon k, n, and the ranges of V/RT_e and C_r considered, we have found crossover points where two V/RT_e values correspond to the same V_a/V, indicating that excellent straight-line plots of log a_j vs T_j^{-1} can be obtained even in the nonequilibrium regime. Second, values of V_a in the nonequilibrium regime will be relatively insensitive to a change in V, i.e., an increase in V (hence, V/RT_e) will reduce V_a/V, leaving V_a much less changed than in either the frozen or equilibrium extremes. One, therefore, expects that the predicted dependence of a_j on T_j in the nonequilibrium regime will be relatively insensitive to the ionization potential of the principal impurity present. As a corollary, for inferring the principal ionizing species, slopes in this regime will be much less useful than slopes in the equilibrium regime.

Comparison with Attenuation Data

The parameters selected in constructing Fig. 2 define a set of conditions approximately met in recent radar attenuation experiments on aluminized, double-base, solid propellant motors,[10, 11] which covered a 650°K range in T_j and nearly a decade range in attenuation. (In keeping with the assumptions underlying Fig. 2, data for chlorine-containing propellants or for nozzle area ratios very different from 8.9 will not be considered here). In Fig. 3 the observed temperature sensitivity of the attenuation is compared, with encouraging results, to that predicted by the present idealized theory. This is done by passing the curve predicted by Eq. (5) through the lowest-temperature data point. For comparison, the much steeper curve (dashed) corresponding to local ionization equilibrium is also shown. In both cases, the impurity is assumed to be sodium ($V = 5.1$ ev), but, in accord with the previous discussion, if the impurity were potassium ($V = 4.3$ ev), slopes computed in the nonequilibrium regime would equally well represent the data. It is not necessary to accurately specify impurity level in this comparison, because the predicted slopes in the nonequilibrium regime are nearly the same over more than a four-decade range of C_r, which, subject to the foregoing assumptions, would correspond to an eight-decade range of impurity level. Of course, the impurity level determines the absolute value of the attenuation.

In correlating data, one must usually account for the fact that attenuation measurements during static firings are made somewhat downstream of the exit plane (to avoid reflections from the nozzle), so that additional expansion (if $p_\infty < p_j$) or compression (if $p_\infty > p_j$) occurs[4] before the observation point is reached. Such corrections can be made on the basis of the flow field determined by the method of characteristics.[12] Peripheral afterburning of fuel-rich exhausts and two-dimensional effects within the nozzle (invalidating simple one-dimensional flow nonequilibrium predictions) can also affect comparisons.[4]

References

[1] Spokes, G. N., "The role of aluminum and its oxides as sources or moderators of electrons in solid propellant rocket exhausts," Stanford Research Institute Rept. TDR 63 326, DDC AD 447 283 (August 1964).

[2] Kurzius, S. C. and Skinner, R. C., "Effects of solid particles on electron concentrations in a plasma," AeroChem TP-72b (March 1964); unclassified section of "Flame plasma effects study," (U), RADC–TDR- 64–263 (October 1964); secret.

[3] Rosner, D. E., "Estimation of electrical conductivity at rocket nozzle exit sections," ARS J. **32**, 1602–1605 (1962).

[4] Rosner, D. E., "Ionization in rocket exhaust plumes," AeroChem TP-85; DDC–AD 447 304 (March 1964); also *Plasma Technology, Aerospace Applications*, edited by J. Grey (Prentice Hall, Inc., Englewood Cliffs, N. J., to be published).

[5] Calcote, H. F., "Relaxation processes in plasma," *Dynamics of Conducting Gases* (Northwestern University Press, Evanston, Ill., 1960), pp. 36–50.

[6] Eschenroeder, A. Q., "Ionization nonequilibrium in expanding flows," ARS J. **32**, 196–203 (1962).

[7] Molmud, P., "Vernier exhaust perturbations on radar and altimeter systems during a lunar landing," AIAA J. **1**, 2816–2819 (1963).

[8] Balwanz, W. W., "Interaction between electromagnetic waves and flames, Part VI: Theoretical plots of absorption, phase shift, and reflection," U. S. Naval Research Lab. NRL Rept. 5388 (September 1959).

[9] Sutton, G. P., *Rocket Propulsion Elements* (John Wiley and Sons, Inc., New York, 1956), 2nd ed.

[10] Vreeland, R. W., unpublished experiments, Allegany Ballistics Lab., Cumberland, Md. (April 5, 1963).

[11] Vreeland, R. W., private communication with H. F. Calcote (November 19, 1963).

[12] Moe, M. M. and Troesch, B. A., "Jet flow with shocks," ARS J. **30**, 487–489 (1960).

Long-Time Room Temperature Tensile Creep Tests of 2014-T6 Aluminum Alloy Used In Titan II

M. J. Brown*

Martin Company, Baltimore, Md.

THE Titan II vehicle is designed to be stored at room temperature with pressurized propellant tanks for from one to three years. This design condition raises the question as to whether significant amounts of creep will occur in bare (unclad) 2014-T6 alloy, with and without welds, when subjected to a stress equivalent to 50% of the ultimate stress, for long periods of time at room temperature. Extrapolation of short-time creep data indicated that the problem was not critical, but confirmation by test was desired.

Material selected for this investigation was obtained from Martin stock in the form of 0.100-in.-thick 2014-T6 bare sheet. All of the specimens were oriented in a direction normal to the rolling direction of the original sheet. The welded specimens were prepared by Titan II manufacturing procedures, using the manual tungsten electrode, A-C inert gas-shielded Tungsten Inert Gas (TIG) method, with 4043 aluminum alloy filler wire. A welding fixture made of a copper backup bar and steel clamping plates was used to ensure properly aligned specimens. The specimens were tested in the as-welded condition (not heat-treated after welding).

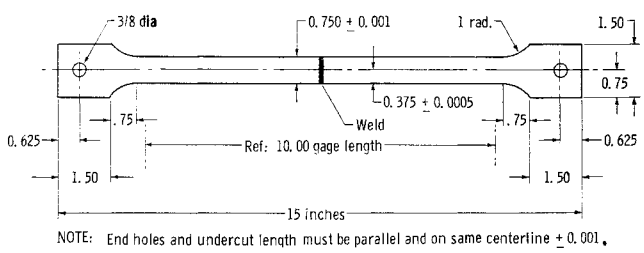

Fig. 1 Test specimen configuration.

Received September 29, 1965; revision received December 14, 1964.

* Supervisor, Materials Engineering, Engineering Laboratories.

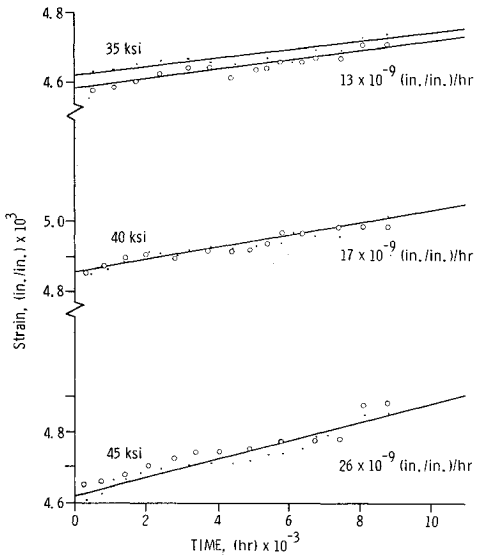

Fig. 2 Creep-unwelded. 2014-T6 bare Al alloy: transverse; room temperature.

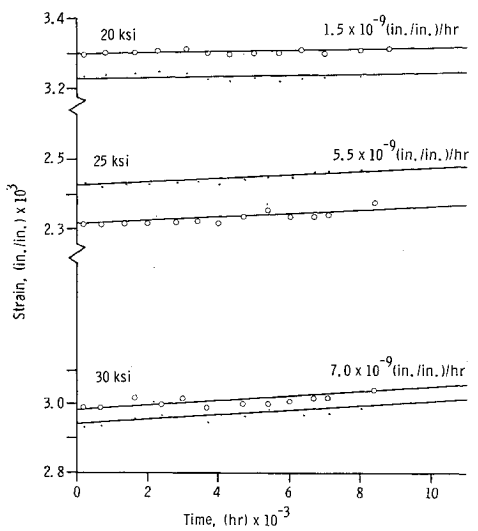

Fig. 3 Creep welds. 2014-T6 bare Al alloy: transverse; room temperature.

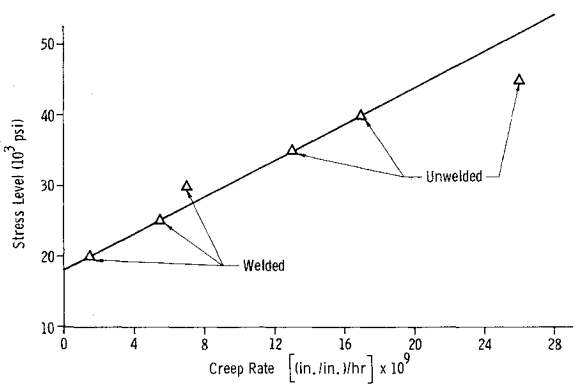

Fig. 4 Creep test data. 2014-T6 Al alloy: transverse; room temperature.

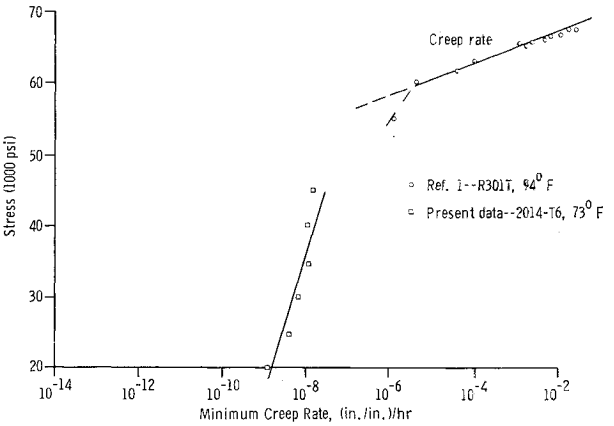

Fig. 5 Creep characteristics.

Test specimens, machined to the configuration shown in Fig. 1, were made 10 in. long to increase the sensitivity of strain measurement; a 10^{-8} (in./in.)/hr measurement capability resulted. The tests were conducted in duplicate, each creep machine containing two specimens loaded in series. Load was applied to the specimen load links by dead weights and a compound lever system. The welded specimens were stressed at 20, 25, and 30 ksi, and the unwelded specimens at 35, 40, and 45 ksi. Strain measurements were obtained with a 100-power telemicroscope providing an accuracy of ± 0.00002 in./in. Periodic readings were made to establish creep curves on each of the 12 test specimens. On completion of the creep test program, stress-strain curves were obtained on the specimens in an air-conditioned laboratory (71°–76°F).

Test Results

Conventional mechanical properties of tensile ultimate (F_{tu}), yield (F_{ty}), and modulus (E) were obtained to establish a relationship for the material strengths before and after a creep stress history. For the basic material specimens control (unwelded), the MIL-HDBK-5, design values of F_{ty} = 57 ksi, F_{tu} = 64 ksi, and $E = 10.4 \times 10^6$ were equalled or exceeded by the test material before and after creep testing (Table 1). The welded controls also exhibited expected values with no significant change after creep testing. These data were obtained in accordance with American Society for Testing Materials (ASTM) Standard E8-46.

The frequency of the creep strain readings was reduced after the first 1000 hr to a reading every two weeks. The

Table 1 Tensile test data and results

Condition	Specimen	F_{ty}, ksi	F_{tu}, ksi	$E \times 10^6$
Basic	A	63.7	73.2	10.3
Material	B	64.3	72.5	10.2
Controls	C	64.3	71.5	10.3
Basic	D	32.5	46.5	10.7
Welded	E	33.9	49.7	10.4
Controls	F	31.1	44.6	10.7
35 ksi[a]	1	63.5	72.5	10.8
Unwelded	2	59.5	68.3	10.8
40 ksi[a]	3	63.9	72.5	10.9
Unwelded	4	63.8	72.1	11.3
45 ksi[a]	5	63.0	65.0	11.0
Unwelded	6	59.6	68.5	10.8
20 ksi[a]	7	33.0	43.0	10.6
Welded	8	30.9	44.1	11.4
25 ksi[a]	9	36.3	47.4	11.6
Welded	10	35.9	48.9	10.9
30 ksi[a]	11	39.4	48.8	10.9
Welded	12	38.7	49.8	10.9

[a] Test coupons were tensile-tested after creep testing.

average slopes are illustrated in Figs. 2 and 3, with corresponding values of creep strain for the full 9000 hr. Undulations are noted which are believed to represent the material response to ambient temperature variations within the error of strain recording. Figure 4 is a composite arrangement of the welded and control specimen data which produces a straight line.

Concluding Discussion

Some of the limited test data available prior to this work were those obtained by Flanigan, Tedson, and Dorn.[1] Their work was conducted on R301-T (clad), which is a clad sheet-metal version of 2014-T6 alloy, at 94°F for times up to 1000 hr. Creep rates from their data of reference and from the present tests are plotted in Fig. 5. The two sets of data, taken together, provide a wide-range picture of the creep performance. The transition between the two portions would be an interesting subject for future investigation. The smallness of the creep strains experienced in these tests leads to the conclusion that creep is not a problem at the temperatures and stresses considered in the Titan II design.

Reference

[1] Flanigan, A. E., Tedson, L. F., and Dorn, J. E., "Stress rupture and creep tests on aluminum alloy sheet at elevated temperatures," American Institute of Mining, Metallurgical, and Petroleum Engineers Tech. Publ. 2033 (November 1946).

Radiation Pressure Torques from Spatial Variations in Surface Properties

ROBERT E. ROBERSON*
University of California, Los Angeles, Calif.

VARIOUS authors have treated the torque on spacecraft from solar radiation pressure, where the torque source arises from the asymmetry of the surface presented to the sun and differential shadowing effects (e.g., Ref. 1). Even when the surface is symmetrical, or at least balanced, with respect to the vehicle center of mass, a torque can exist because of differential reflectivity of surface elements and variations in the direction of the surface normal, both caused by local surface irregularities. These are statistical effects and may tend to average to zero over the entire vehicle. Nevertheless, there is a nonzero probability of torque magnitude different from zero. The purpose of this note is to develop the probability density function for torque components from this source.

With reference to Fig. 1, let zero be any base point used for the calculation of torque, e.g., the vehicle center of mass. Let $\{\mathbf{e}_\alpha\}$ ($\alpha = 1, 2, 3$) be a set of unit base vectors embedded in the vehicle with origin at O, and denote by S_i a surface element whose area is ΔA_i and whose unit normal vector is $\mathbf{n}_i$. S_i is located with respect to O by vector $\mathbf{r}_i$. Discrete, not infinitesimal areas, are considered here; the physical model corresponding to this assumption is an array of solar cells whose properties might reasonably be assumed constant but statistically different from those of neighboring cells. The argument is generalized in a straightforward way to a surface with continuous properties, in which case ΔA_i, in the analysis below, can be interpreted simply as the characteristic sizes of surface areas over which reflectivity and surface normal are substantially constant. Denote by $\mathbf{E}$ the unit vector in the direction of incident radiation, the same for all surface elements, and by $\mathbf{R}_i$ the unit vector in the direction of the net reflected momentum. It is supposed that $\mathbf{E}$, $\mathbf{n}_i$, and $\mathbf{R}_i$ are coplanar with angles $\langle \mathbf{E}, \mathbf{n}_i \rangle = \pi - \alpha_i$, $\langle \mathbf{n}_i, \mathbf{R}_i \rangle = \alpha_i'$. The angles α_i and α_i' need not be equal, if one assumes that the area ΔA_i itself has minute variations in surface normal that cause diffuse reflection. However, it is assumed here that, although the various $\mathbf{n}_i$ may differ among themselves, the reflection from any one area element is specular so that $\alpha_i' = \alpha_i$.

Take the incident radiation pressure to be P_0 (units of dynes/square centimeter, say) and the effective pressure of the reflected radiation momentum from element i to be $\eta_i P_0$, where η_i is a coefficient $0 \leq \eta_i \leq 1$ describing reflectivities from zero (complete absorption) to complete reflection. Noting that the projections of ΔA_i normal to $\mathbf{E}$ and $\mathbf{R}_i$ are $\Delta A_i \cos\alpha_i$ and $\Delta A_i \cos\alpha_i'$, respectively, it is evident that the torque about O of forces on ΔA_i is

$$\mathbf{L}_i = \mathbf{r}_i \times [P_0 \Delta A_i \cos\alpha_i \mathbf{E} + \eta_i P_0 \Delta A_i \cos\alpha_i'(-\mathbf{R}_i)] \quad (1)$$

Since $\mathbf{R}_i$, $\mathbf{E}$, and $\mathbf{n}_i$ are coplanar,

$$\mathbf{R}_i = \mathbf{E} + 2\cos\alpha_i \mathbf{n}_i \quad (2)$$

where the equality of α_i and α_i' has been used. Hence,

$$\mathbf{L} = P_0 \sum_i \Delta A_i \mathbf{r}_i \times [(1 - \eta_i)\cos\alpha_i \mathbf{E} - 2\eta_i \cos^2\alpha_i \mathbf{n}_i] \quad (3)$$

The scalar component of torque is found by introducing†

$$\mathbf{L} = L_\beta \mathbf{e}_\beta \qquad \mathbf{r}_i = r_{i\beta}\mathbf{e}_\beta \qquad \mathbf{E} = E_\beta \mathbf{e}_\beta \qquad \mathbf{n}_i = n_{i\beta}\mathbf{e}_\beta$$

There is no loss in generality in supposing $\mathbf{e}_3$ coincident with $-\mathbf{E}$, so that $E_\beta = -\delta_{3\beta}$. Then,

$$L_\beta = -P_0 \epsilon_{\beta\lambda\mu} \sum_i \Delta A_i r_{i\lambda}[(1 - \eta_i)\cos\alpha_i \delta_{3\mu} + 2\eta_i \cos^2\alpha_i n_{i\mu}] \quad (4)$$

Effects of Surface Variations

Suppose that η_i^*, α_i^*, and $\mathbf{n}_i^*$ are nominal values of η_i, α_i, and $\mathbf{n}_i$ such that, if these nominal values hold, the torque components $L_\beta = 0$. Here, we are concerned only with such *nominally balanced systems*: nominal unbalance can be treated separately by conventional methods. Suppose further that *actual* values of η_i, α_i, and $\mathbf{n}_i$ are

$$\eta_i = \eta_i^* + \delta\eta_i \qquad \alpha_i = \alpha_i^* + \delta\alpha_i$$
$$\mathbf{n}_i = \mathbf{n}_i^* + \delta\mathbf{n}_i$$

Note that $\delta\mathbf{n}_i$ is not arbitrary, since both $\mathbf{n}_i$ and $\mathbf{n}_i^*$ are unit vectors: thus $2\delta\mathbf{n}_i \cdot \mathbf{n}_i^* + |\delta\mathbf{n}_i|^2 = 0$. Nor is it independent

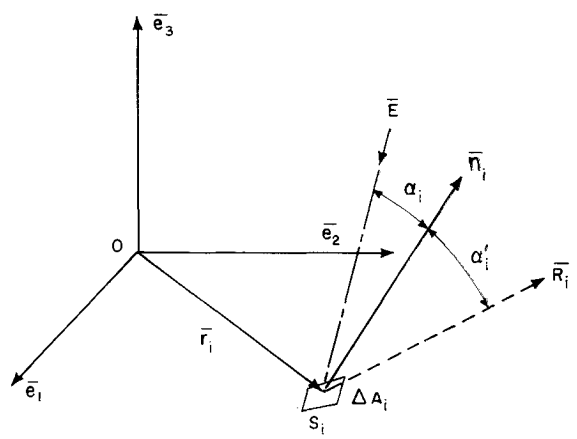

Fig. 1 Correlation of transition to turbulent flow in hypersonic wakes behind blunt bodies.

Received December 4, 1964.

* Professor of Engineering. Associate Fellow Member AIAA.

† The summation convention is used for Greek indices that have the range 1, 2, 3; Latin indices range over all of the surface elements, and the summation sign is included explicitly.